New Journal of Physics
An Institute of Physics and Deutsche Physikalische Gesellschaft Journal

Subsequent layer growth of supported nanoparticles by deposition of Sb_4 clusters onto $MoS_2(0001)$

B Stegemann, B Kaiser and K Rademann
Institut für Chemie, Humboldt-Universität zu Berlin, Brook-Taylor-Str 2, D-12489 Berlin, Germany
E-mail: bernhard.kaiser@chemie.hu-berlin.de

New Journal of Physics **4** (2002) 89.1–89.10 (http://www.njp.org/)
Received 1 August 2002, in final form 18 October 2002
Published 11 November 2002

Abstract. The surface morphology after deposition of Sb_4 clusters onto $MoS_2(0001)$ at 90 K has been studied in detail with scanning tunnelling microscopy in ultrahigh vacuum. It has been found that during the initial stage of growth two-dimensional nanoparticles are formed. With increasing coverage these nanoparticles grow layer by layer and each layer has the height of one monolayer of undissociated Sb_4 clusters. The interface width (surface roughness) has been quantitatively determined as a function of total coverage. Ideal three-dimensional layer-by-layer growth has been identified for the single particles according to a Poisson distribution of exposed areas of the layers of the particles. Consequently, antimony grows on $MoS_2(0001)$ without interlayer diffusion which is suppressed by an effective step edge (Schwoebel–Ehrlich) barrier.

1. Introduction

The controlled formation and manipulation of well-defined nanostructured surfaces by the deposition of size-selected clusters has attracted significant attention recently [1]–[4]. The properties of the nanostructures depend decisively on the morphology of the system. One central goal of current studies is to relate the nonequilibrium growth mode to the underlying atomic deposition and diffusion mechanisms [5, 6]. In principle, by understanding these elementary mechanisms one could tailor the morphologies and thus the properties of the desired material.

Sb_4 is a stable molecular cluster which can easily be obtained in large amounts by evaporating solid antimony under ultrahigh vacuum (UHV) conditions. We have shown previously that Sb_4 clusters can be utilized as precursors for the assembly of well-ordered nanostructured surfaces with a wide range of distinct morphologies [7]–[9]. Furthermore, antimony thin films and

1367-2630/02/000089+10$30.00

supported nanoparticles are known to undergo a phase transition from amorphous to crystalline under various experimental conditions [9]–[14]. Phase transitions strongly modify structural and electronic properties of the particles. Thus, antimony nanoparticles provide intriguing opportunities for exploring size-dependent properties. Layered or pyramid-shaped nanoparticles are here of special interest, since they allow the investigation of the change in the properties as a function of the number of atomic layers [15]. Therefore, the successful preparation of suitable nanoparticles with well-defined dimensions at the atomic scale and the development of methods to produce such samples are very important issues.

The layer-by-layer growth of islands and nanoparticles has been investigated for metal homoepitaxial systems [16]–[19] and heteroepitaxial systems [20, 21]. In either case the morphology of the system at given substrate temperature and particle flux is decisively determined by the diffusion coefficient and the step edge barrier for interlayer transport E_S (Schwoebel–Ehrlich barrier) [22, 23]. Besides kinetic parameters the growth process in heteroepitaxial systems might also be influenced by a lattice mismatch at the interface.

In this study we have applied scanning tunnelling microscopy (STM) to investigate the growth kinetics of thermally deposited Sb_4 clusters onto the basal (0001) plane of MoS_2. The MoS_2(0001) plane is a weakly interacting surface, which had been held at a temperature of 90 K during deposition in order to reduce the mobility of the Sb_4 clusters. The investigation presented here focuses mainly on the shape and morphology of the evolving antimony nanoparticles. It is demonstrated that by choosing appropriate deposition conditions, the controlled formation of nanoparticles by subsequent layer growth is feasible. From a detailed characterization of the morphology we deduce associated mass-transport processes and discuss the influence of the diffusion barrier E_S at the step edges on the growth mode.

2. Experimental details

The experiments have been performed in two directly coupled stainless steel UHV chambers. The first chamber contains the tools for sample preparation, the second chamber a Beetle-type STM [24] for surface analysis. The base pressure in the preparation chamber is 2×10^{-10} mbar, in the STM chamber 4×10^{-11} mbar. Samples have been transferred to the STM without breaking the vacuum. STM analysis is performed at room temperature and all STM data have been acquired in the constant current mode using electrochemically etched tungsten tips. The STM images are greyscale topographs, where darker regions generally indicate lower heights, except for figure 2(a), which is a differentiated image (‘illuminated from the left’).

As substrates we have used MoS_2 single crystals in the form of natural mineral molybdenite obtained from JEOL Europe. MoS_2 has a layer structure and is composed of S–Mo–S sandwiches, which are weakly bound to each other by van der Waals forces, providing an easy cleavage plane of the crystal. Clean surfaces are easily obtained by cleaving in air with adhesive tape. The cleaving procedure removes the top few layers of S–Mo–S stacking sheets leaving large, atomically flat terraces with (0001) orientation. After immediate transfer into the UHV chamber the sample had been heated for about 2 h at 550 °C to desorb atmospheric adsorbates, i.e. mainly water.

Antimony of 99.9999% purity from Johnson–Matthey has been deposited by thermal evaporation from a Knudsen cell at a typical temperature of 330 °C onto the MoS_2(0001) surface. During deposition the substrate had been cooled with liquid nitrogen and held at a temperature of 90 K. The deposition rate can be varied over several orders of magnitude by adjusting the

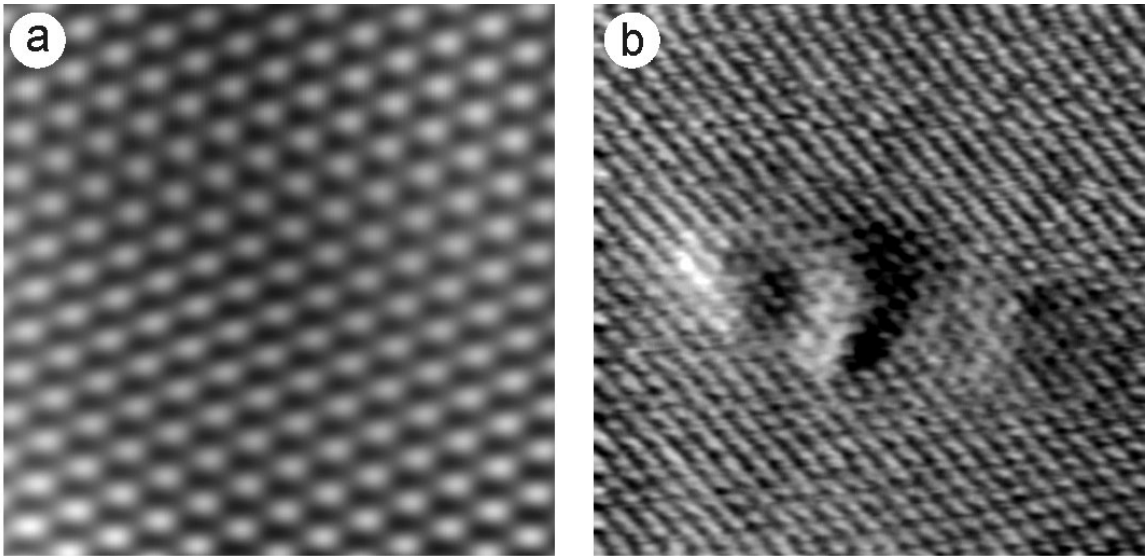

Figure 1. (a) STM image (39×39 Å^2) of the bare, atomically resolved $MoS_2(0001)$ surface, exhibiting the hexagonal lattice of the sulfur atoms in the top plane. A low-pass FFT filter has been applied in order to minimize noise. (b) STM image (78×78 Å^2) of a ring-like structure on the MoS_2 basal plane attributed to an impurity ion intercalated between the MoS_2 layers. Tunnelling parameters: (a) 0.20 V, 2.0 nA, (b) 0.16 V, 1.0 nA.

source temperature and has been monitored by measuring the frequency shift of a movable, water-cooled quartz microbalance. Additionally, coverages have been determined directly from the STM images. The vapour phase of antimony consists exclusively of the molecular clusters of Sb_4 at the applied temperature [25], so that truly monodisperse particles are deposited with thermal energies. All coverages are given in monolayers (ML), where 1 ML corresponds to the equivalent of a monomolecular layer of Sb_4 clusters. The deposition rate used in this study was 0.15 ML min^{-1}.

3. Results

3.1. The bare $MoS_2(0001)$ surface

Before deposition the bare $MoS_2(0001)$ surface exhibits large terraces, which are atomically flat and thus suitable for studying the results of the deposition process. The lateral extension of these terraces is typically larger than 1 μm and exceeds the maximum scanning width of the STM (0.5 μm). Stepped regions, which form the boundaries of the terraces are found just in a minority of STM images. STM images with atomic resolution of the clean $MoS_2(0001)$ surface yield a hexagonal symmetry with a lattice constant of 3.16 Å (see figure 1(a)). As the tunnelling conditions were chosen such that the STM tip was sufficiently far from the surface, the protrusions can be ascribed to the sulfur atoms in the top plane of MoS_2 [26].

Though typically the terraces have been found to be atomically flat, a few defect structures have been observed on the surface. Examining these defects in detail reveals protrusions and ring-like structures very similar to previous observations [27]–[29]. Figure 1(b) shows

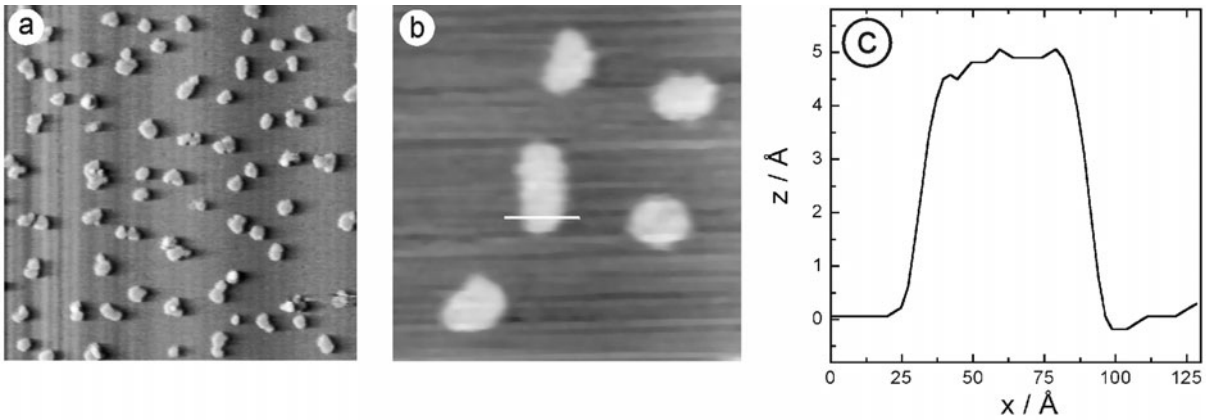

Figure 2. (a) Differentiated STM image (2480×2480 Å^2) of the surface morphology after deposition of 0.10 ML of Sb_4 clusters. (b) STM image (620×620 Å^2) of the formed nanoparticles in detail. Tunnelling parameters: -1.7 mV, 0.9 nA. (c) Cross-section of a nanoparticle, corresponding to the white line in (b).

such a defect structure. These structures are attributed to electronic effects of intercalated impurity ions (e.g. vanadium, fluoride), which are interstitially located in the molybdenum layer, rather than to adsorbates on the surface [28]. This interpretation is supported by atomic force microscopy (AFM) studies, which revealed a perfect lattice of sulfur atoms without defects or adsorbates [30].

3.2. Formation of single-layer particles

The surface morphology after deposition of antimony has been studied systematically from the submonolayer range up to a few MLs. In general, tunnelling conditions for stable imaging of the obtained nanostructures turned out to be rather delicate. At small tip–sample distances the scanning motion of the STM tip easily manipulates the nanoparticles. Most ideal conditions have been achieved at about -1.8 V and 1.0 nA, typically. After deposition of small amounts of Sb_4 such as 0.10 ML, small two-dimensional nanoparticles are created which have not been observed on the bare $MoS_2(0001)$ surface and which must hence be formed by diffusion and aggregation of Sb_4 clusters. Figure 2(a) shows a typical STM micrograph of the surface morphology. An enlarged view of an ensemble of a few nanoparticles is shown in figure 2(b). A cross-section of a particle corresponding to the white line is plotted in figure 2(c). This graph shows that the nanoparticles have a typical height of nearly 5 Å and an average diameter of about 70 Å. Statistical image analysis gives a number density of 1.2×10^{10} particles cm^{-2}.

3.3. Growth of subsequent layers

Increasing the total coverage of Sb_4 clusters leads to a change in the growth morphology. Figure 3(a) shows an STM image of the surface after deposition of 0.22 ML. Not only are single-layer particles formed, but particles consisting of two layers are also found. Nucleation in the second layer has already started on the particles long before the first layer is completed (see figure 3(b)). This observation indicates the existence of a step edge barrier hindering interlayer

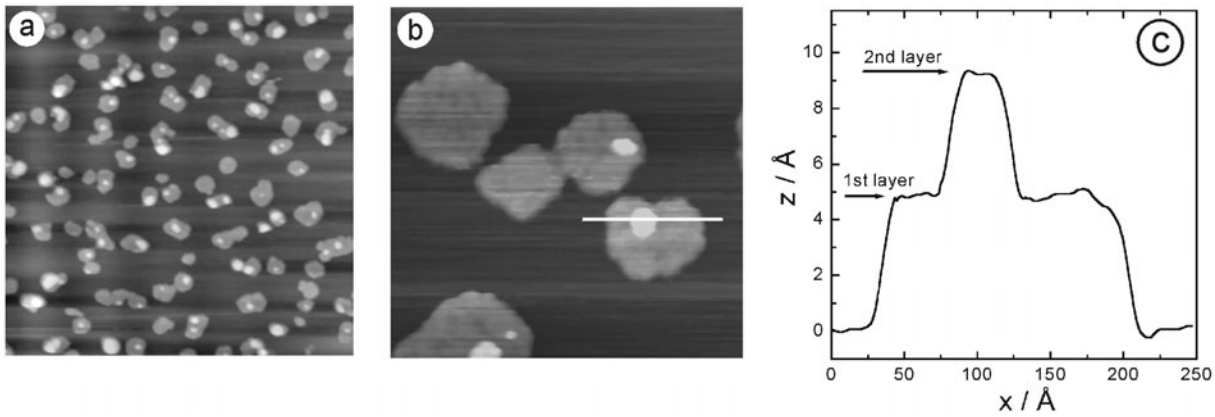

Figure 3. (a) STM image (2480×2480 Å^2) of the surface morphology after deposition of 0.22 ML of Sb_4 clusters. (b) STM image detail (620×620 Å^2) of the nanoparticles formed. Tunnelling parameters: -2.0 mV, 1.0 nA. (c) Cross-section of a nanoparticle, corresponding to the white line in (b).

mass-transport. From the cross-section in figure 3(c) the height of the second layer is measured to be nearly 5 Å, thus equalling the height of the first layer. Moreover, the lateral size of the bottom layer of the particles has increased to about 120 Å. The number density as determined from statistical analysis yields 1.5×10^{10} particles cm^{-2}.

Further increase of the total coverage leads to a growth of both the first and the second layer of the particles. Overviews of the surface morphology after deposition of 0.28 and 0.62 ML are shown in figures 4(a) and (b), respectively. In these images a few examples are found where particles have already coalesced. Figure 4(c) shows the transition from nanoparticles consisting of one or two layers to nanoparticles with up to three layers at a coverage of 0.83 ML. It is clearly seen that compared with the particles in figures 4(a) and (b) nucleation in the third layer is found for most of the nanoparticles at 0.83 ML. Increasing the coverage to 1.3 ML (shown in figure 5) leads to the continued growth of all layers resulting in stacked particles. The thickness of these nanoparticles ranges from one to three individual layers. The cross-section plot in figure 5(c) reveals that each layer has a height of 4.5–5.0 Å. The bottom layers of the particles are no longer well separated. At higher coverage coalescence of the first layer becomes dominant.

4. Discussion

From the STM characterization of the surface morphology the main processes leading to the growth of the nanoparticles can be identified as follows: (i) deposition on a terrace, (ii) diffusion on a terrace, (iii) nucleation, (iv) attachment at particles and aggregation, (v) deposition on top of a particle. The particles are evenly distributed over the surface. No preferential step decoration is observed. Thus, growth at existing step edges of the support is of minor importance. The possible influence of the point defects of the substrate (see figure 1(b)) on the particle number density has been elucidated by varying the evaporation flux. As discussed in section 3.2 a coverage of 0.10 ML Sb_4 deposited with a rate of 0.15 ML min^{-1} yields a number density of 1.2×10^{10} particles cm^{-2}. Increasing the deposition rate by a factor of 10 (1.5 ML min^{-1}) leads to a number density of 1.6×10^{10} particles cm^{-2}. The average number of intrinsic point defects

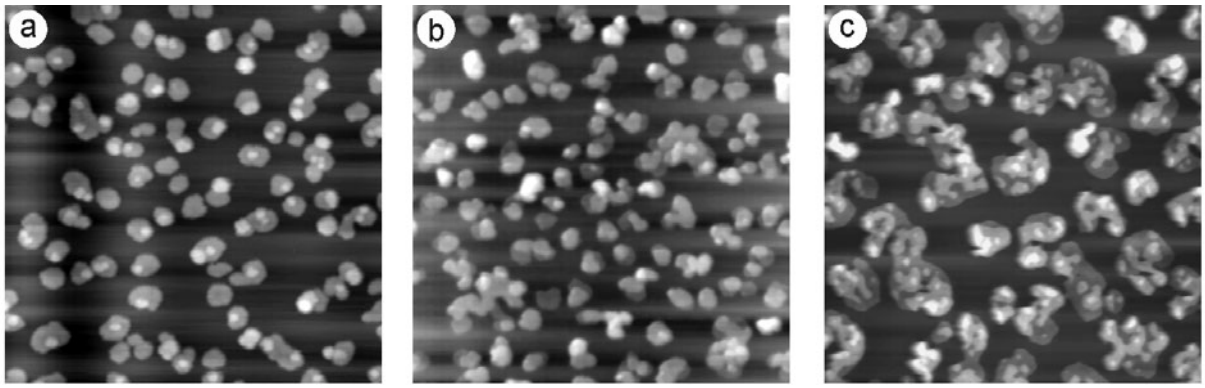

Figure 4. STM images (2480×2480 Å^2) of the surface morphology after deposition of (a) 0.28 ML, (b) 0.62 ML and (c) 0.83 ML of Sb_4 clusters. Tunnelling parameters: (a) 1.5 mV, 1.0 nA; (b) -1.2 mV, 1.1 nA; (c) -2.5 mV, 1.0 nA.

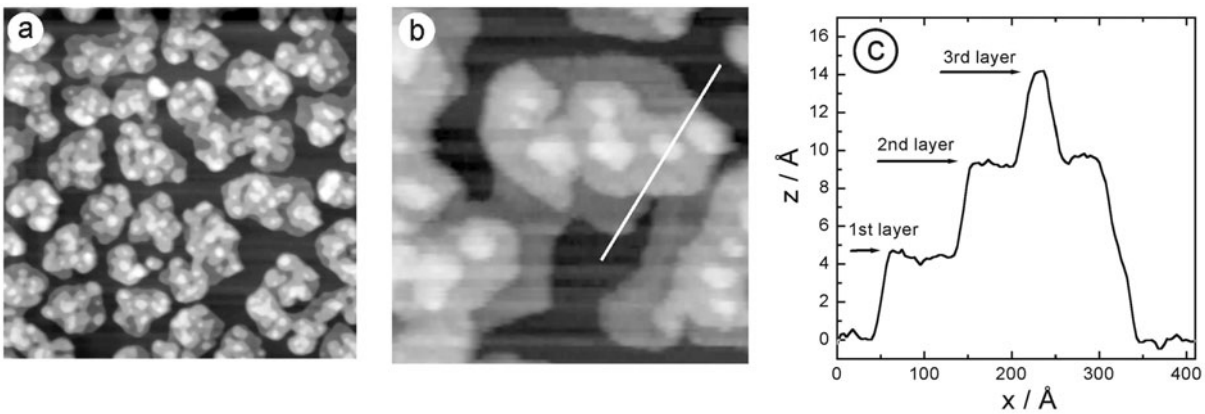

Figure 5. (a) STM image (2480×2480 Å^2) of the surface morphology after deposition of 1.3 ML of Sb_4 clusters. (b) STM image detail (620×620 Å^2) of the nanoparticles formed. Tunnelling parameters: -1.5 mV, 1.0 nA. (c) Cross-section of a nanoparticle, corresponding to the white line in (b).

found on the $MoS_2(0001)$ surface (see figure 1(b)) is usually less than 2×10^9 particles cm^{-2} and hence significantly lower. These intrinsic defects may act as nucleation centres for subsequent growth processes, but from the comparably low number density we infer that this growth mode is not dominant. We conclude that homogeneous nucleation is active, i.e. stable particles are dominantly formed by aggregation of diffusing Sb_4 clusters.

4.1. Interpretation of the height of the layers

It is known that the surface temperature during deposition strongly influences the resulting growth mode [6]. At the low substrate temperature of 90 K the mobility of the deposited Sb_4 clusters on MoS_2 is clearly reduced. According to our data there is no general epitaxial relation between the particle orientation and the substrate lattice. Therefore, the growth is considered to

be mainly a result of kinetic limitations. As all STM data have been taken at room temperature even though deposition was done at 90 K, the images do not necessarily reflect the situation immediately after deposition. Changes may have occurred upon warming the samples up to room temperature. However, at room temperature the deposition of Sb_4 on $MoS_2(0001)$ clearly results in very different particle sizes and shapes. In the initial growth stage three-dimensional, disc-shaped nanoparticles with a lateral diameter of up to 120 nm and a height of up to 40 nm are formed due to the higher mobility of the Sb_4 clusters. This morphology is very similar to the growth behaviour of Sb_4 on the (0001) plane of highly oriented pyrolytic graphite (HOPG) [9].

The presented cross-sections of the layered particles reveal that all layers are of equal height, each corresponding to a value of 4.5–5.0 Å. This height is in coincidence with the size of the deposited Sb_4 clusters and will be discussed in the context of the properties of Sb_4 in the following.

The gas phase of antimony consists of Sb_4 clusters [25]. There is no macroscopic solid phase of antimony composed of tetramers (comparable to white phosphorus P_{4n} or yellow arsenic As_{4n}) [31]. However, in rather disordered amorphous films three-dimensional crystalline regions consisting of undissociated Sb_4 clusters have been observed on $MoS_2(0001)$ and on $AuSb_2(100)$ [8]. These well ordered regions are of nearly cubic symmetry with lattice constants in the range of 4.27 Å and 5.06 Å, matching the height of the layers. Furthermore, the special stability of individual Sb_4 clusters has been demonstrated in the gas phase [32] and on silicon surfaces [33]. According to these results, we exclude a possible collision-induced dissociation of Sb_4 during thermal deposition and assume a survival of Sb_4 on the surface after deposition. Sb_4 has a regular tetrahedral structure [34] with a bond length as determined by *ab initio* calculations of $a = 5.08$ au [35]. It is known that STM images do not resolve any internal features of Sb_4 clusters on surfaces. Instead, a superposition of the four atoms of the tetrahedral cluster is observed as a single protrusion with well-defined height and lateral extension of nearly 5 Å [33]. The measured heights of the antimony layers of 4.5–5.0 Å in our measurements are in good agreement with all these data and cannot be explained by the lattice parameters of crystalline α-antimony [31]. Therefore, we conclude that each layer of the particles is assembled from Sb_4 clusters, as they were deposited. Regarding the kinetic processes, Sb_4 clusters can indeed be considered to be the elementary particles in this system, which do not dissociate but rather diffuse and aggregate on the surface to form two-dimensional particles with compact shapes and monomolecular height. However, no discrete Sb_4 units or any regular arrangement in the layered particles could be resolved.

4.2. Analysis of surface roughness

Besides the information on the step heights of the particles, statistical data about the lateral properties of each layer have been extracted from the STM images. Due to the finite tip size it has to be taken into account that the particle size may be overestimated in the STM images, and the deposit seems to cover a larger fraction on the substrate. In order to circumvent this problem, the total deposited amount as measured with the quartz microbalance has been compared with the total coverages determined from STM images. Additionally, different STM tips have been used for image acquisition. As a result, the values agree within an error of less than 10%.

From statistical analysis of the particle sizes we inferred quantitative data about the partial amount of material contained in each individual layer $P(i, \Theta)$ at a certain total coverage Θ. The parameter i refers to the layer number counting from the support surface. Thus $i = 0$

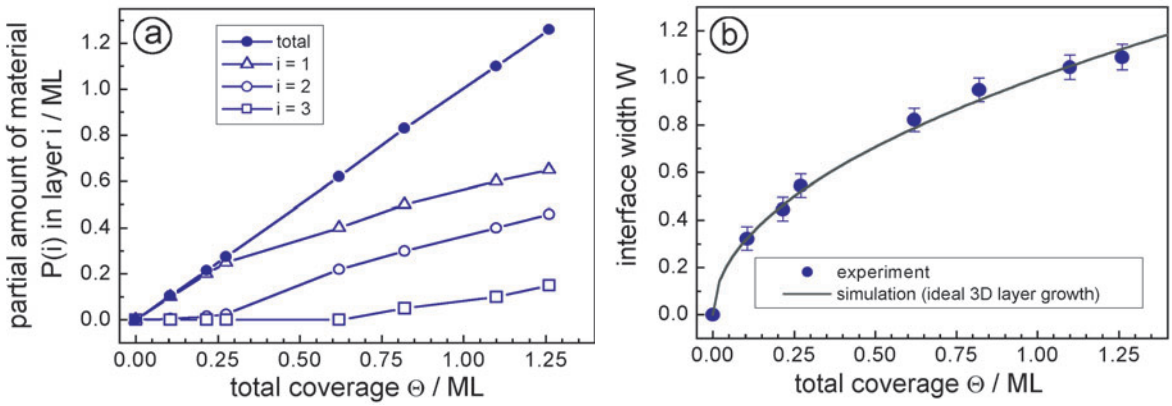

Figure 6. (a) Partial amount of antimony found in the first layer (open triangles), in the second layer (open circles) and in the third layer (open squares) of the particles as the function of coverage. The total deposited amount, resulting from the sum of the material in all layers, is given in full circles. (b) Interface width as a function of coverage as determined from equation (1). The solid curve corresponds to an ideal three-dimensional layer growth without step diffusion assuming a Poisson distribution of net exposed areas of the layers (see equation (3)).

corresponds to the support surface, $i = 1$ to the first antimony layer, and so on. The plot in figure 6(a) summarizes the results of this analysis and gives the partial amount of material found to be in the first layer (open triangles), in the second layer (open circles) and in the third layer (open squares) of the particles as a function of coverage. Nucleation in the fourth layer turns out to be negligible even at $\Theta = 1.3$ ML. The total deposited amount, resulting from the sum of the material in all layers, is given in full circles. It is seen that above coverages of 0.28 ML significant growth of the second layer is initiated, whereas the onset of third-layer growth appears above 0.62 ML.

In order to characterize quantitatively the growth morphology of the particles at a certain total coverage we consider in the following the interface width W. This parameter characterizes the surface roughness and depends on the net exposed area $N(i, \Theta)$ in each individual layer as follows [36]:

$$W^2 = \sum_{i=0}^{\infty} (i - \Theta)^2 N(i, \Theta). \tag{1}$$

The first factor in the sum of this equation accounts for the deviation from ideal layer-by-layer growth. Thus, small exposed areas in upper layers contribute to the surface roughness and account considerably to the interface width.

The interface width is decisively determined by the interlayer mass-transport. Ideal two-dimensional layer-by-layer growth requires the absence of a step edge barrier ($E_S = 0$) and thus a permanent interlayer transport of all particles arriving on top of existing particles. Each time a layer is completely closed (i.e. Θ is an integer number) the interface width yields $W = 0$. In contrast, an ideal three-dimensional particle growth is obtained in the case of an infinite step edge barrier ($E_S = \propto$). All deposited particles stay at the level where they arrive. Thus, no interlayer mass-transport takes place, which leads to the formation of particles on top of other

particles. The number of layers increases with increasing coverage. This mode is called Poisson random deposition growth [37], since it was shown that under these conditions the net exposed areas $N(i, \Theta)$ of the individual layers i of the particles follow a Poisson distribution [38]:

$$N(i, \Theta) = \frac{\Theta^i}{i!} \mathrm{e}^{-\Theta}. \tag{2}$$

Substituting $N(i, \Theta)$ in equation (1) yields the relation [39]

$$W^2 = \Theta. \tag{3}$$

According to these considerations the interface width covers a range of $0 < W < \sqrt{\Theta}$ for the entire range of step edge barriers $0 < E_S < \infty$. However, in special cases of non-ideal behaviour W may even exceed $\sqrt{\Theta}$ as a result of upward mass-transport [40], or ideal three-dimensional growth can be weakened even at infinite step edge barrier due to various effects directly related to the deposition process, like funnelling, transient mobility or knockout mechanisms [36].

The net exposed areas $N(i, \Theta)$ and, accordingly, the interface width W have been determined for all investigated coverages. The obtained data points are plotted in figure 6(b). In addition, the behaviour for an ideal three-dimensional layer growth according to equation (3) is drawn as a solid line. It can be seen clearly that the simulated curve of ideal three-dimensional layer growth fits the experimental data points very well within the experimental error. From this agreement it is concluded that the observed particles grow according to a Poisson distribution and hence possess a high activation barrier for downward diffusion. This barrier effectively prevents interlayer mass-transport and determines the observed three-dimensional layer-by-layer growth mode.

5. Summary

The surface morphology and the growth behaviour of thin antimony films on the basal plane of MoS_2 have been investigated by STM in UHV. The films with a thickness between 0.1 and 2.0 ML have been prepared by thermal deposition of monodisperse Sb_4 clusters. Deposition has been carried out at a substrate temperature of 90 K. All STM images have been taken at room temperature. The morphology of the system depends on the substrate temperature and the deposition parameters. It has been demonstrated that nanometre-sized particles are formed on terraces of the $MoS_2(0001)$ surface. In the initial stage of growth these particles are formed by a two-dimensional layer. With increasing coverage nucleation on top of the first and the second layer begins, long before the first layer is completed. Therefore, the overall growth mode is three-dimensional (Volmer–Weber type) and not layer by layer. As all layers are of equal height (4.5–5.0 Å), corresponding to the diameter of an Sb_4 unit, we conclude that the layers consist of undissociated Sb_4 clusters. The interface width has been determined as a function of coverage in order to characterize quantitatively the growth characteristics of the particles and to explain the particle shapes. The obtained data can be fitted very well using a Poisson distribution of exposed layer areas. Thus, the particles grow in an ideal three-dimensional mode. As a consequence, the observed growth mode can be explained by the existence of a step edge barrier, which prevents downward diffusion.

Acknowledgments

BS wishes to thank B Wendling for stimulating discussions. Financial support by the Deutsche Forschungsgemeinschaft (DFG) is gratefully acknowledged.

References

[1] Meiwes-Broer K H 2000 *Metal Clusters at Surfaces: Structure, Quantum Properties, Physical Chemistry (Springer Series in Cluster Physics)* (Berlin: Springer)
[2] Jensen P 1999 *Rev. Mod. Phys.* **71** 1695
[3] Binns C 2001 *Surf. Sci. Rep.* **44** 1
[4] Moriarty P 2001 *Rep. Prog. Phys.* **64** 297
[5] Zhang Z and Lagally M G 1997 *Science* **276** 377
[6] Brune H 1998 *Surf. Sci. Rep.* **31** 125
[7] Stegemann B, Bernhardt T M, Kaiser B and Rademann K 2002 *Surf. Sci.* **511** 153
[8] Bernhardt T M, Stegemann B, Kaiser B and Rademann K 2002 *Angew. Chem.* at press
[9] Kaiser B, Stegemann B, Kaukel H and Rademann K 2002 *Surf. Sci.* **496** L18
[10] Lotmar W 1945 *Helv. Phys. Acta* **18** 369
[11] Hashimoto M, Sugibuchi H and Kambe K 1982 *Thin Solid Films* **98** 197
[12] Fuchs G, Melinon P, Aires F S, Treilleux M, Cabaud B and Hoareau A 1991 *Phys. Rev.* B **44** 3926
[13] Nakai T, Sagawa K, Nakada T, Saito Y and Kaito C 2000 *Phys. Low-Dim. Struct.* **11/12** 101
[14] Brechignac C, Cahuzac P, Carlier F, Colliex C, de Frutos M, Kebaili N, Le Roux J, Mason A and Yoon B 2001 *Eur. Phys. J.* D **16** 265
[15] Schintke S, Messerli S, Pivetta M, Patthey F, Libioulle L, Stengel M, De Vita A and Schneider W-D 2001 *Phys. Rev. Lett.* **87** 276801
[16] Tersoff J, Vandergon A W D and Tromp R M 1994 *Phys. Rev. Lett.* **72** 266
[17] Bartelt M C and Evans J W 1995 *Phys. Rev. Lett.* **75** 4250
[18] Esch S, Breeman M, Morgenstern M, Michely T and Comsa G 1996 *Surf. Sci.* **365** 187
[19] Kohler U, Jensen C, Wolf C, Schindler A C, Brendel L and Wolf D E 2000 *Surf. Sci.* **454** 676
[20] Zeng H and Vidali G 1995 *Phys. Rev. Lett.* **74** 582
[21] Canepa M, Terreni S, Cantini P, Campora A and Mattera L 1997 *Phys. Rev.* B **56** 4233
[22] Schwoebel R L and Shipsey E J 1966 *J. Appl. Phys.* **37** 3682
[23] Ehrlich G and Hudda F G 1966 *J. Chem. Phys.* **44** 1039
[24] Besocke K 1987 *Surf. Sci.* **181** 145
[25] Mühlbach J, Pfau P, Recknagel E and Sattler K 1981 *Surf. Sci.* **106** 18
[26] Altibelli A, Joachim C and Sautet P 1996 *Surf. Sci.* **367** 209
[27] Heckl W M, Ohnesorge F, Binnig G, Specht M and Hashimi M 1991 *J. Vac. Sci. Technol.* B **9** 1072
[28] Permana H, Lee S and Simon Ng K Y 1992 *J. Vac. Sci. Technol.* B **10** 2297
[29] Kushmerick J G, Kandel S A, Han P, Johnson J A and Weiss P S 2000 *J. Phys. Chem.* B **104** 2980
[30] Ha J S, Roh H S, Park S J, Yi J Y and Lee E H 1994 *Surf. Sci.* **315** 62
[31] Donohue J 1974 *The Structures of the Elements* (New York: Wiley)
[32] Kaiser B, Bernhardt T M, Stegemann B, Opitz J and Rademann K 1999 *Phys. Rev. Lett.* **83** 2918
[33] Mo Y W 1994 *J. Vac. Sci. Technol.* B **12** 2231
[34] Sontag H and Weber R 1982 *Chem. Phys.* **70** 23
[35] Kumar V 1993 *Phys. Rev.* B **48** 8470
[36] Evans J W 1991 *Phys. Rev.* B **43** 3897
[37] Trofimov V I, Mokerov V G and Shumyankov A G 1997 *Thin Solid Films* **306** 105
[38] Poelsema B and Comsa G 1990 *Phys. Rev.* B **41** 11609
[39] Evans J W, Sanders D E, Thiel P A and DePristo A E 1990 *Phys. Rev.* B **41** 5410
[40] Voigtländer B 2001 *Surf. Sci. Rep.* **43** 127